Results: Mass

Luke Chamandy

November 20, 2017

1 Intro

We present results from run 132. This run has softening length $2.4\,\mathrm{R}_\odot = 1.7 \times 10^{11}$ cm, and smallest resolution element of $0.14\,\mathrm{R}_\odot = 9.8 \times 10^9$ cm.

2 Mass accretion

2.1 Krumholz mass accretion

Krumholze-type accretion was implemented in the code for all of run 132 for the companion (P2). The RG core (P1) was set to "no accretion." Results are shown in Fig. 1.

2.2 Mass accumulation around P1 and P2

For the same simulation with Krumholz accretion for P2 and no accretion for P1, we integrated the mass inside a sphere centered at P1 or P2. Results are shown in the top and bottom panels of Fig. 2 for P2 and P1, respectively, as well as in Fig. 3, for larger choices of the sphere radius r_s. The case $r_\mathrm{s} = 7 \times 10^{10}$ cm is shown in both figures to enable easier comparison.

2.3 Comparison with literature

Our system consists of a RG of radius 3.35×10^{12} cm, mass of $1.96\,\mathrm{M}_\odot$, and particle core mass of $0.37\,\mathrm{M}_\odot$, along with a particle companion of mass $0.98\,\mathrm{M}_\odot$, initialized in a circular orbit at an orbital separation 3.41×10^{12} cm. We do not initialize the RG with a spin. Our softening length is 1.7×10^{11} cm. We compare parameter values of run 132 with parameter values of Ricker & Taam and Ohlmann et al. (2016) in Tab. 1 and 2.

2.3.1 Ricker & Taam

Ricker & Taam (2008, 2012) performed one simulation with smallest resolution element exactly twice as large as our smallest (we are effectively using 4096^3 near the point particles whereas they effectively used 2048^3 since they had the same simulation box size). Their system consisted of a RG of radius 2.2×10^{12} cm, mass of $1.05\,\mathrm{M}_\odot$, and particle cloud core with radius 6×10^{10} cm and mass of $0.36\,\mathrm{M}_\odot$, along with a particle cloud companion of cloud radius 6×10^{10} cm and mass $0.6\,\mathrm{M}_\odot$, initialized in a circular orbit at an orbital separation 4.3×10^{12} cm. They initialized the RG with a spin of 95% of the synchronous rate.

Ricker & Taam calculated the mass accretion by integrating the mass flux through a spherical "control surface." Their results for the mass accretion are shown in Fig. 4. They also calculated the mass evolution assuming a Bondi-Hoyle-Lyttleton rate (thin lines, but the rate is divided by 100 to fit in the figure).

2.4 Mass accretion rates

In Tab. 3 we show the maximum and average accretion rates obtained over the course of our simulation ($t = 0$ to $t = 68.3$ d), and also show the average rate obtained by Ricker & Taam (2012) from $t = 20$ d to the end of their simulation at $t = 57$ d (labelled with superscript 'RT'). We chose $t = 20$ d because this seems to be roughly when the

Table 1: Comparison of masses, ambient density, and initial spin for our run 132 and that of Ricker & Taam (2008, 2012). Initial mass of red giant M_RG, mass of red giant core m_1, initial mass of companion m_2, constant ambient density ρ_amb, Initial (solid-body) rotation rate Ω_i.

Model	$M_\mathrm{RG}[\mathrm{M}_\odot]$	$m_1[\mathrm{M}_\odot]$	$m_2[\mathrm{M}_\odot]$	Accretion m_1	Accretion m_2	ρ_amb [g cm^{-3}]	Ω_i
Run 132	1.96	0.37	0.98	None	Krumholz	6.7×10^{-9}	0
Ricker & Taam	1.05	0.36	0.6	None	None	10^{-9}	$0.95\Omega_\mathrm{K}$
Ohlmann et al. at $t = 0$	1.98	0.38	0.99	None	None	2×10^{-10}	$0.95\Omega_\mathrm{K}$

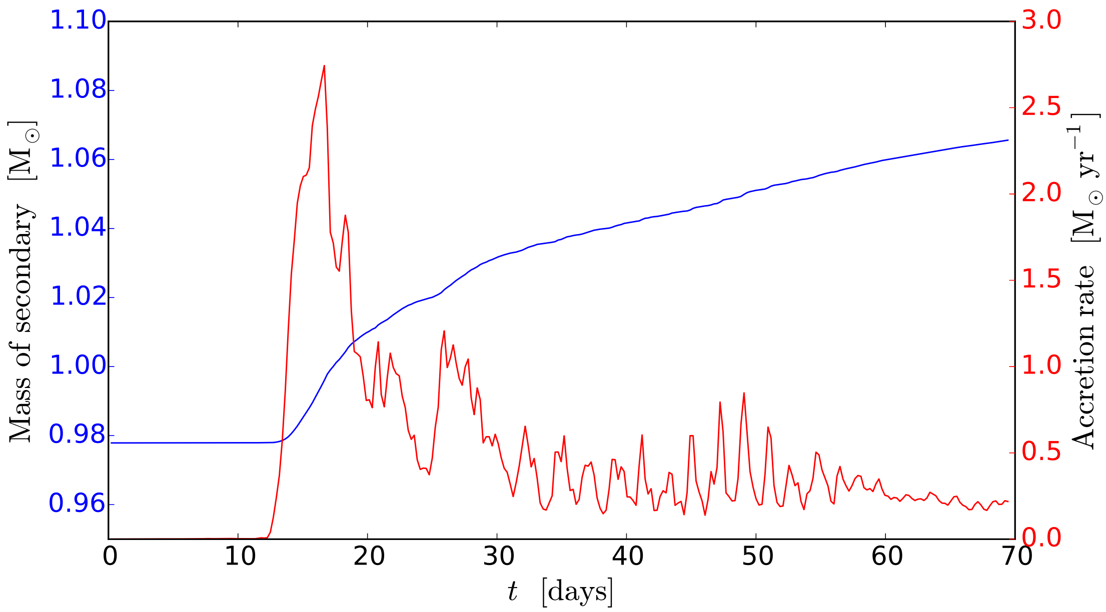

Figure 1: Mass of companion P2 obtained directly from simulation output (Krumholz accretion). Cumulative mass (blue) and accretion rate (red) obtained by numerical differentiation of the cumulative mass.

Table 2: Comparison of lengths for our run 132 and that of Ricker & Taam (2008, 2012). Red giant radius $R_{\rm RG}$, effective particle or cloud radius $R_{\rm p}$, initial inter-particle separation $a_{\rm i}$, smallest resolution element Δ_x, and simulation box dimension $L_{\rm box}$. Parameter values for Ohlmann et al. (2016) given for $t=0$ but changed thereafter.

Model	$R_{\rm RG}$[cm]	$R_{\rm p}$[cm]	$a_{\rm i}$[cm]	particle type	Δ_x[cm]	$L_{\rm box}$ [cm]
Run 132	3.35×10^{12}	1.7×10^{11}	3.41×10^{12}	single	9.8×10^{9}	4×10^{13}
Ricker & Taam	2.2×10^{12}	6×10^{10}	4.3×10^{12}	$N=2\times10^{5}$ cloud	2×10^{10}	4×10^{13}
Ohlmann et al. at $t=0$	$\sim3.35\times10^{12}$	1.9×10^{11}	$\sim3.41\times10^{12}$	single	9.8×10^{9}	3.3×10^{14}

plunge in starts, but actually the number is quite arbitrary. For the smaller values of $r_{\rm s}$ (which Ricker & Taam 2012 say are the most reliable values) the accretion rate changes only mildly during most of the simulation so the choice of the initial time would not make a very large difference to the average mass accretion rate, and here we are making order of magnitude comparisons.

In Tab. 4 we present the results for the Bondi-Hoyle-Lyttleton accretion rate, calculated internally in our simulation using the Krumholz et al. (2004) algorithm. A similar method was used (without allowing any actual change in the mass of the companion particle cloud) by Ricker & Taam (2012), and their results are also included in Tab. 4.

2.5 Discussion

- It is not really correct to compare directly the values we obtain with those obtained by Ricker & Taam, especially with regard to the companion, since we had accretion turned on in the simulation.
- Our softening radius is 1.7×10^{11} cm, effectively the particle radius for both particles, whereas they use a particle cloud with radius 6×10^{10} cm for both RG core and companion. It may not be justified to make the control radius smaller than the effective particle radius.
- Our accretion rates increase as the control radius is increased, but are quite consistent in their qualitative behaviour with time (e.g. whether the slope is positive or negative at a given time). By contrast, results of Ricker & Taam (2012) for different control radii show stronger qualitative differences.
- Nevertheless, like them we find that the BHL rate is orders of magnitude larger than the rate determined using a spherical control surface (for $r_{\rm s}=3.5\times10^{10}$ cm we obtain a factor 6×10^{3}, whereas they obtained a factor 4×10^{2}).
- We obtain a negative value of the accretion rate onto the RG core for all control radii, whereas Ricker & Taam obtained positive values for 3.5×10^{10} cm and 7×10^{10} cm.

3 Mass budget

The evolution of the mass of the various components of the system is presented in Fig 5.

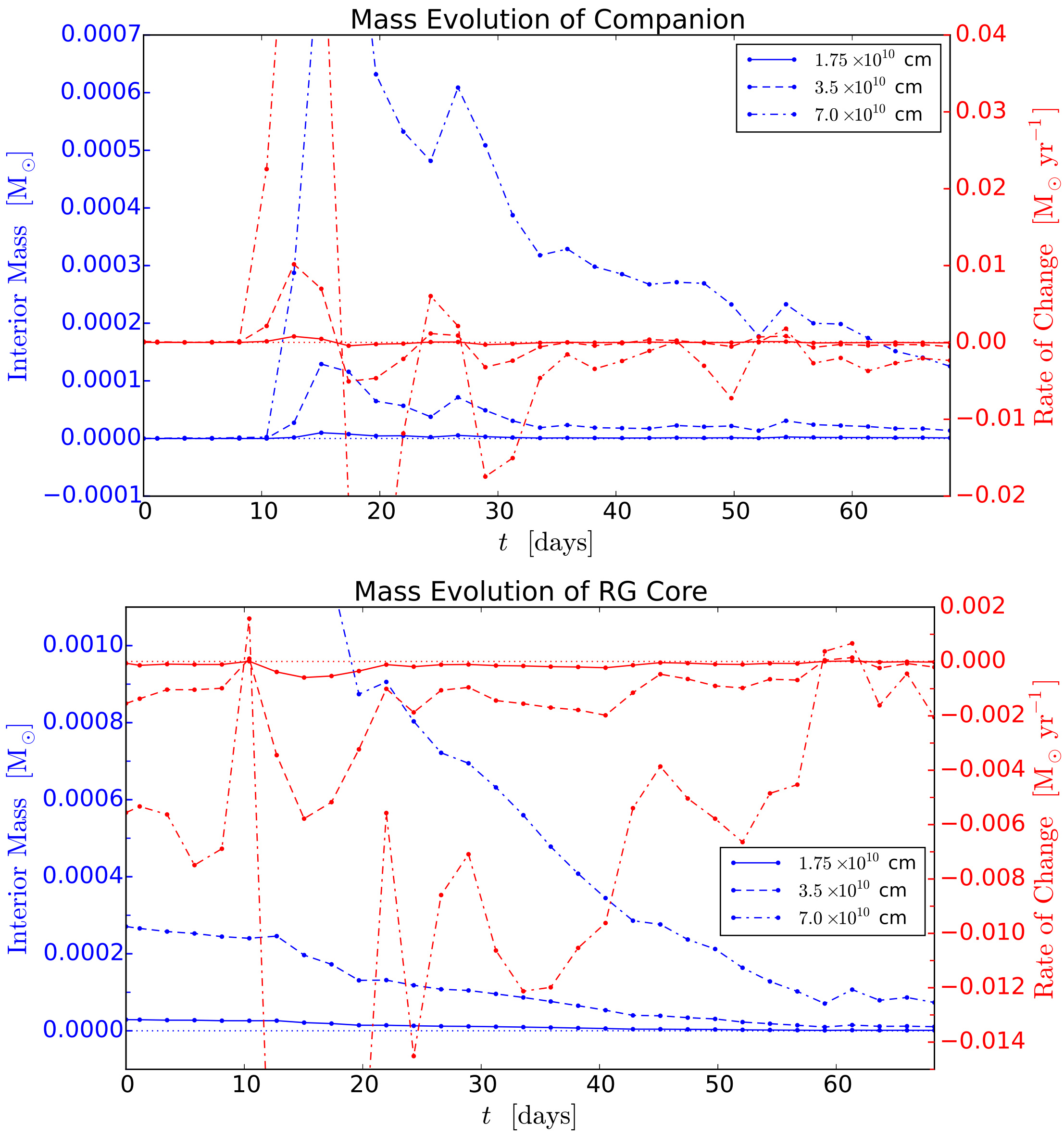

Figure 2: Mass interior to the sphere (blue) and rate of change (red) obtained by numerical differentiation of the interior mass. Choices of radii for 'control spheres' are relatively small. Top: Mass inside spheres of different radii, for companion P2. Bottom: Mass inside spheres of different radii, for RG core P1.

Table 3: Comparison of accretion rates from this work and Ricker & Taam (2012). Accretion rates are determined by differentiation of the mass interior to the sphere with respect to time. Subscript 's' refers stands for 'sphere.' Superscript 'RT' refers to Ricker & Taam (2012), while quantities without superscript refer to this work (run 132). Angular brackets refer to the mean value in the time interval 0–68.3 d (run 132) or 20–57 d (Ricker & Taam, 2012). For run 132 we also show the maximum values of the accretion rate.

Particle	r_s [10^{10} cm]	max($\dot{M}_s$) [$M_\odot$ yr^{-1}]	$\langle \dot{M}_s \rangle$ [$M_\odot$ yr^{-1}]	$\langle \dot{M}_s^{RT} \rangle$ [$M_\odot$ yr^{-1}]
RG core	1.75	2×10^{-5}	-1×10^{-4}	–
RG core	3.5	1×10^{-4}	-1×10^{-3}	0.05
RG core	7	2×10^{-3}	-1×10^{-2}	0.04
RG core	14	2×10^{-2}	-5×10^{-2}	−0.07
RG core	21	8×10^{-2}	-1×10^{-1}	< -0.08
Companion	1.75	8×10^{-4}	5×10^{-6}	–
Companion	3.5	1×10^{-2}	7×10^{-5}	0.01
Companion	7	7×10^{-2}	7×10^{-4}	0.01
Companion	14	3×10^{-1}	3×10^{-3}	0.02
Companion	21	7×10^{-1}	8×10^{-3}	0.03

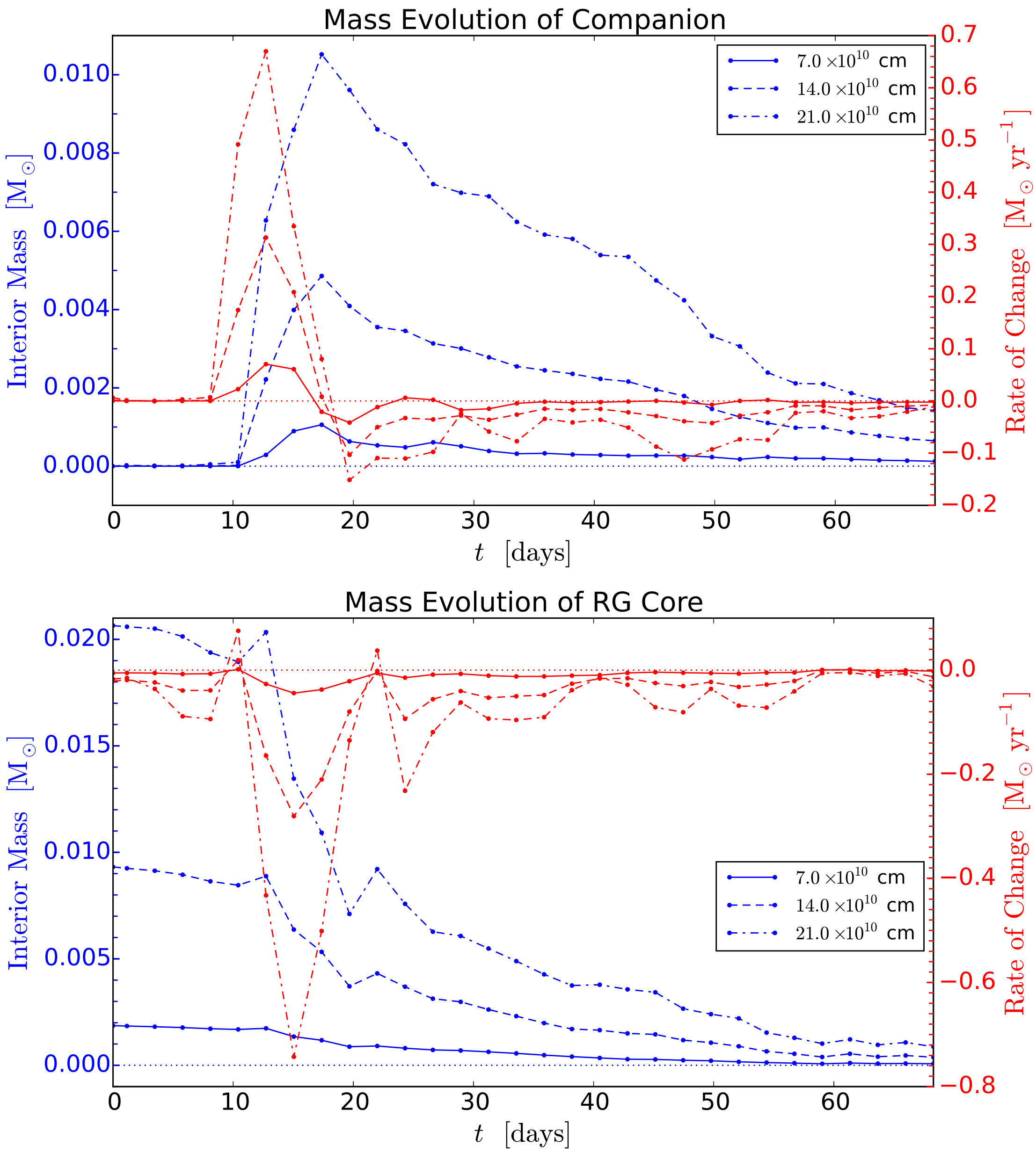

Figure 3: Same as Fig. 2 but for a larger set of control radii. Note that $r_s = 7 \times 10^{10}$ cm is plotted in this figure and in Fig. 2 for easy comparison.

Table 4: Comparison of Bondi-Hoyle-Lyttleton (BHL) accretion rates between our work and Ricker & Taam (2012), and comparison of BHL rates with rates from the method using spherical control surfaces. Here we take $r_s = 3.5 \times 10^{10}$ cm. Superscript 'RT' refers to Ricker & Taam (2012), while quantities without superscript refer to this work (run 132).

Particle	$\max(\dot{M}_{\rm BHL})\,[{\rm M}_\odot\,{\rm yr}^{-1}]$	$\langle\dot{M}_{\rm BHL}\rangle\,[{\rm M}_\odot\,{\rm yr}^{-1}]$	$\langle\dot{M}^{\rm RT}_{\rm BHL}\rangle\,[{\rm M}_\odot\,{\rm yr}^{-1}]$	$\langle\dot{M}_{\rm BHL}\rangle/\langle\dot{M}_{\rm s}\rangle$	$\langle\dot{M}^{\rm RT}_{\rm BHL}\rangle/\langle\dot{M}^{\rm RT}_{\rm s}\rangle$
RG Core	–	–	14.	–	3×10^2
Companion	2.7	0.46	4.	6×10^3	4×10^2

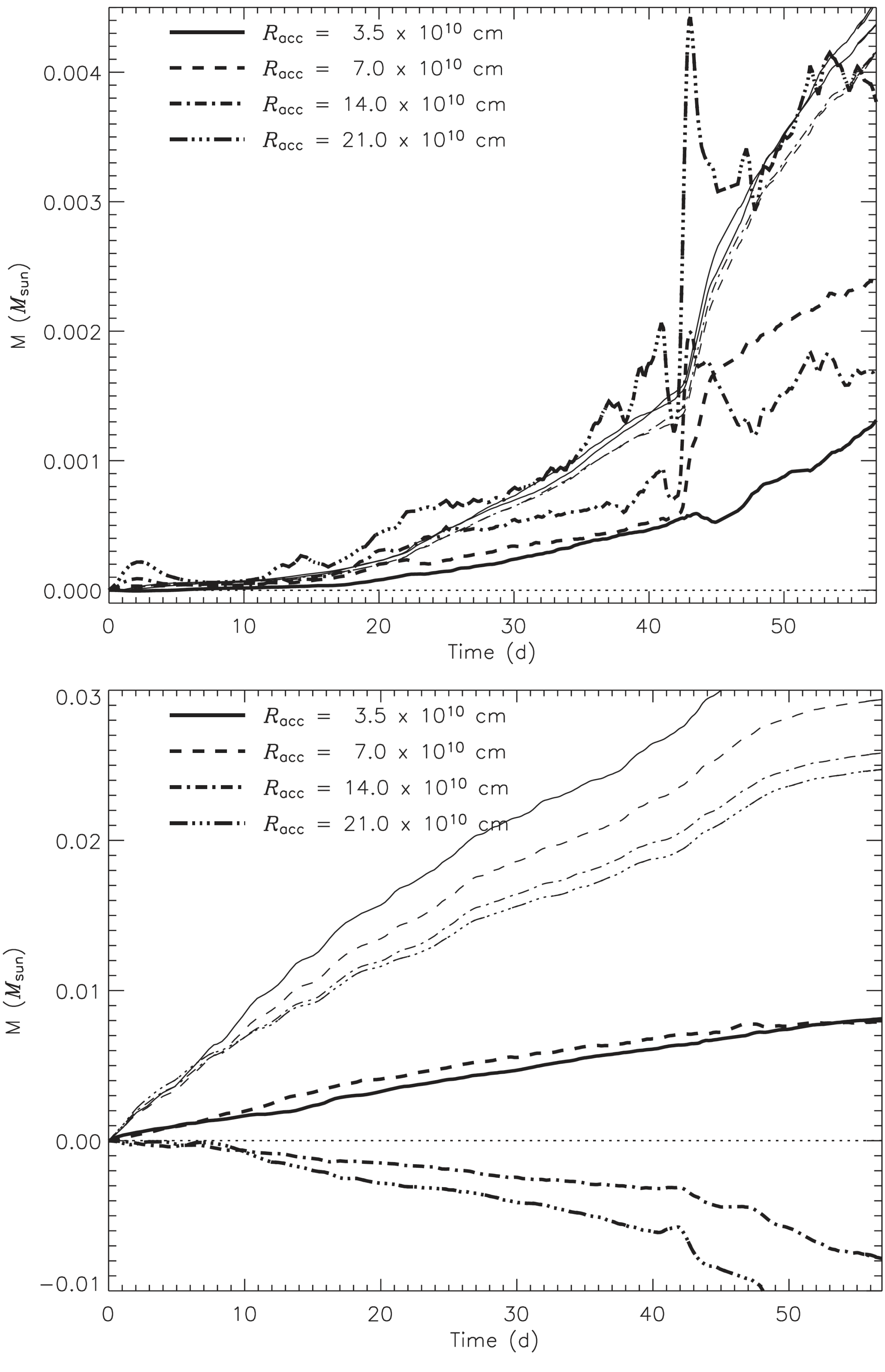

Figure 4: Fig. 5 of Ricker & Taam (2012) for the companion (top) and RG core (bottom). Note that they start their companion farther away from the RG surface than we do at $t = 0$. "Thin curves show the accreted mass as determined using the BHL model from density, pressure, and velocity averages within the same control surfaces, **divided by 100**."

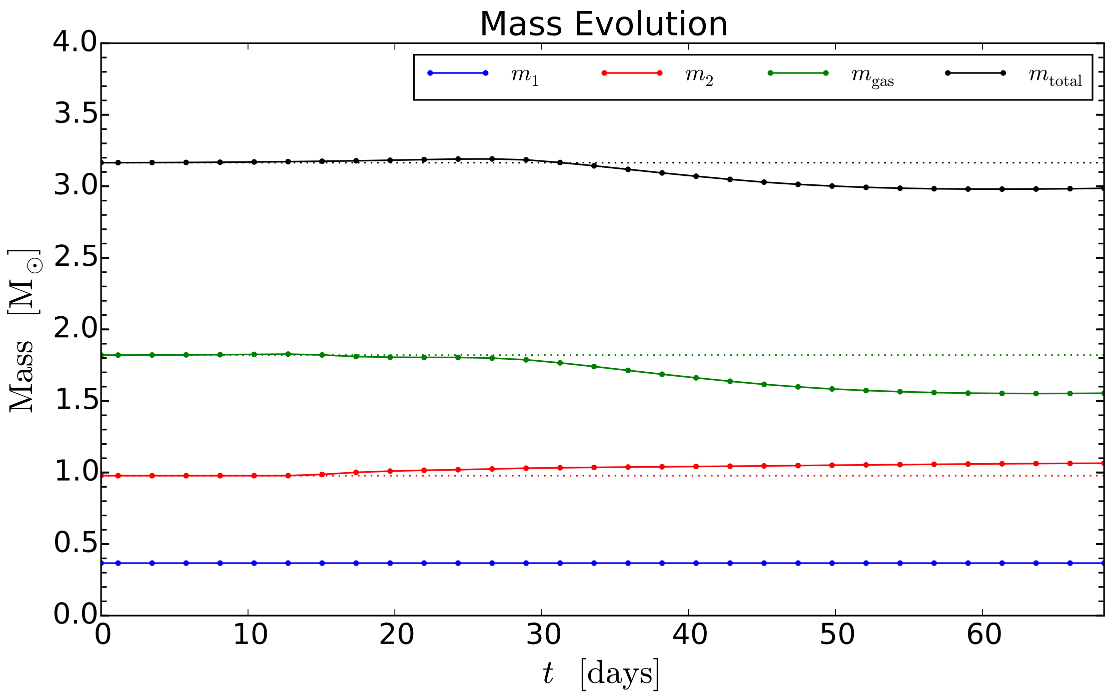

Figure 5: Evolution of the mass budget with time. Total mass in black, gas mass in green, RG core mass in blue, and companion mass in red.

- We see that the total mass first increases slightly and then decreases, before levelling off. The early increase in the first $\sim 10\,\mathrm{d}$ coincides with an increase in the mass of gas m_{g}, and must be caused by inflow from the boundaries. Inflow occurs because the ambient medium is initially uniform, and left on its own, it tries to establish hydrostatic equilibrium by way of a mass flux toward the RGB star.
- From $t \sim 10$–$25\,\mathrm{d}$ the gas mass decreases even as the total mass is still rising, presumably because the rate of mass accretion onto the companion becomes greater than the rate of inflow from the boundaries.
- The gas mass and total mass then decrease more rapidly from about $t = 25\,\mathrm{d}$ to $t = 55\,\mathrm{d}$. This must be caused by material leaving the box through the boundaries.
- Finally, by about 55 d, the masses of all components start to level off. This is caused by the orbit stabilizing, so that material is no longer driven outward toward the boundaries, and accretion onto the companion is also low as the companion is no longer spiralling inward, and so does not encouter 'new' gas.

4 Center of mass

In Figs. 6 and 7 we plot the center of mass for the various components: particles (violet), gas (green), gas+RG core (yellow), and total system of gas+particles (black). Fig. 6 shows the evolution in the xy plane while Fig. 7 shows the evolution with respect to the z axis.

- The CM of the system remains within about $1\,\mathrm{R}_\odot$ from its starting point until $t \sim 30\,\mathrm{d}$, when it suddenly starts to drift.
- The direction of drift is approximately along the vector $(1, 1, 0)$, though there is small drift in the direction of positive z as well, which starts a little later than the drift in x and y.
- Up until $t \sim 30\,\mathrm{d}$, the CM of particles and that of gas both traveled some $\sim 10\ \mathrm{R}_\odot$ from their origins, but the CM of the system had not moved very much.
- After $t \sim 30\,\mathrm{d}$, the particles seem to become 'uncoupled' from the gas.
- At 68 d, the CM of the system has traveled about $20\,\mathrm{R}_\odot$ from its starting point, and is decellerating. This can be compared with the box dimension of $575\,\mathrm{R}_\odot$.

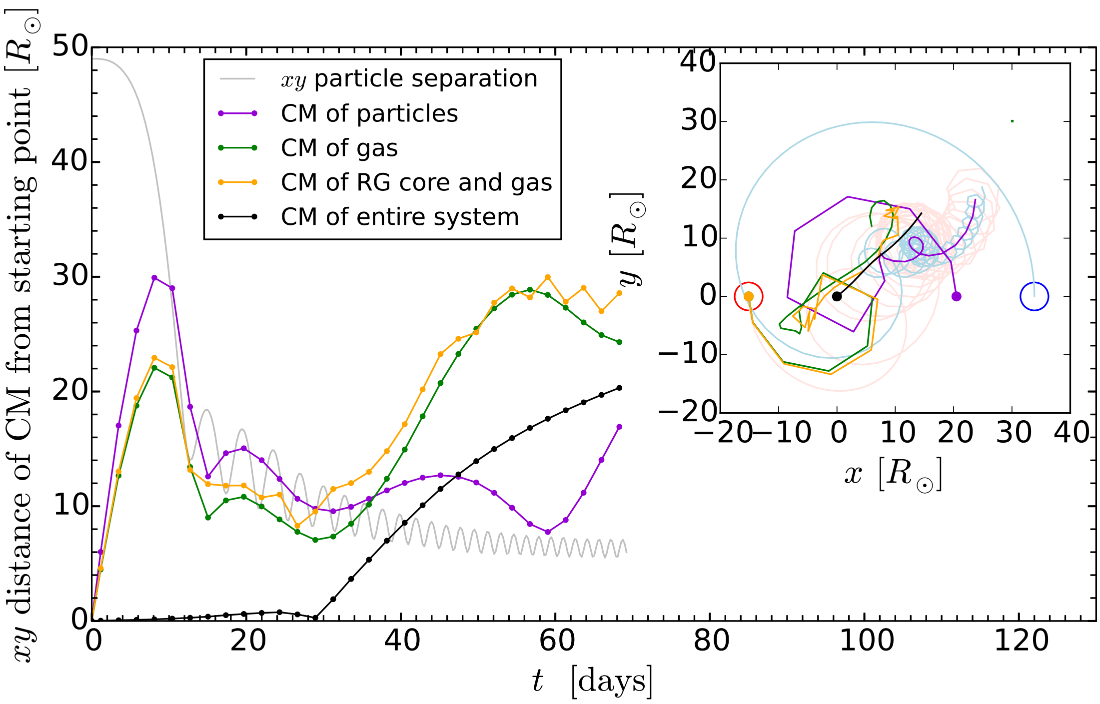

Figure 6: Center of mass: distance traveled from starting point, and path projected onto the xy-plane (inset).

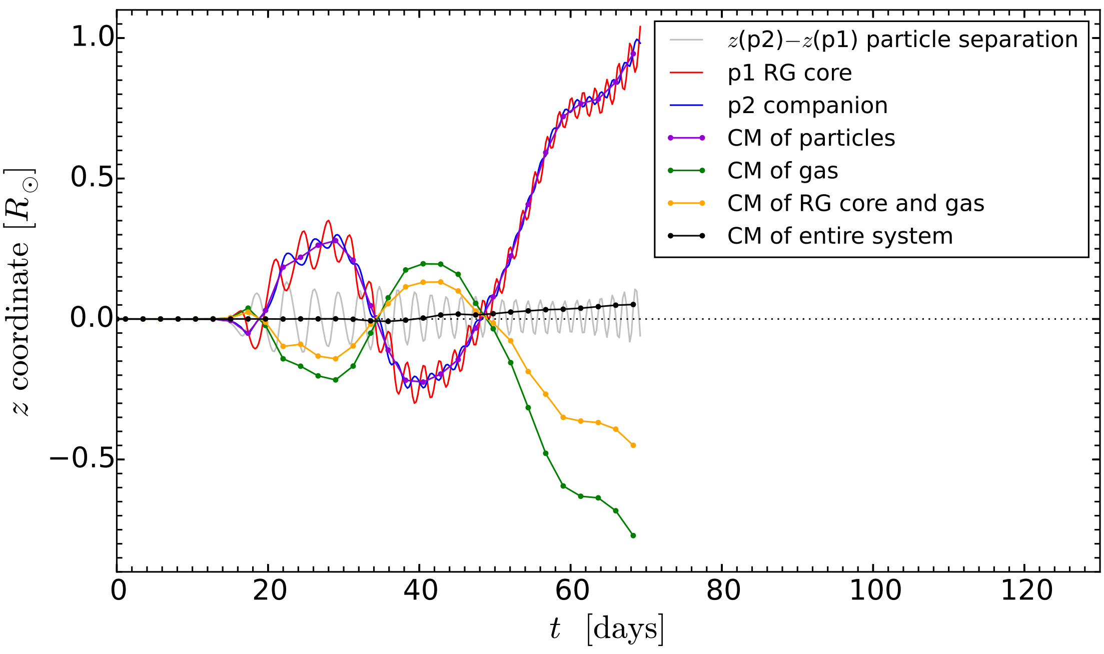

Figure 7: z-coordinate of center of mass.

References

Krumholz, M. R., McKee, C. F., & Klein, R. I. 2004, ApJ, 611, 399

Ohlmann, S. T., Röpke, F. K., Pakmor, R., & Springel, V. 2016, ApJ, 816, L9

Ricker, P. M., & Taam, R. E. 2008, ApJ, 672, L41

—. 2012, ApJ, 746, 74